

1-14-2004

# Dense nonaqueous phase liquid (DNAPL) source zone characterization: Influence of hydraulic property correlation on predictions of DNAPL infiltration and entrapment

Lawrence D. Lemke

*University of Michigan - Ann Arbor*, ap3968@wayne.edu

Linda M. Abriola

*University of Michigan - Ann Arbor*

Pierre Goovaerts

*Biomedware, Inc.*

---

## Recommended Citation

Lemke, L. D., L. M. Abriola, and P. Goovaerts (2004), Dense nonaqueous phase liquid (DNAPL) source zone characterization: Influence of hydraulic property correlation on predictions of DNAPL infiltration and entrapment, *Water Resour. Res.*, 40, W01511, doi:[10.1029/2003WR001980](https://doi.org/10.1029/2003WR001980).

Available at: <http://digitalcommons.wayne.edu/geofrp/16>

NOTICE IN COMPLIANCE WITH PUBLISHER POLICY: An edited version of this paper was published by AGU. Copyright © 2004 American Geophysical Union. Available at: <http://dx.doi.org/10.1029/2003WR001980>

# Dense nonaqueous phase liquid (DNAPL) source zone characterization: Influence of hydraulic property correlation on predictions of DNAPL infiltration and entrapment

Lawrence D. Lemke<sup>1</sup> and Linda M. Abriola

Department of Civil and Environmental Engineering, University of Michigan, Ann Arbor, Michigan, USA

Pierre Goovaerts

Biomedware, Inc., Ann Arbor, Michigan, USA

Received 10 January 2003; revised 4 August 2003; accepted 9 October 2003; published 14 January 2004.

[1] The influence of aquifer property correlation on multiphase fluid migration and entrapment was explored through the use of correlated and uncorrelated porosity, permeability, and capillary pressure-saturation ( $P_c$ -Sat) parameter fields in a cross-sectional numerical multiphase flow model. Data collected from core samples in a nonuniform sandy aquifer were used to generate three-dimensional aquifer parameter fields. Porosity was assumed to be uniform or simulated using sequential Gaussian simulation (SGS). Permeability ( $k$ ) was modeled independently of porosity using SGS as well as simulated geostatistical indicator classes derived from measured grain size distribution curves. Retention characteristics were assigned employing Leverett scaling of a representative  $P_c$ -Sat curve to the geostatistical  $k$  fields or, alternatively, on the basis of simulated indicator classes and porosity values. Ensemble dense nonaqueous phase liquid (DNAPL) infiltration and entrapment behavior for a hypothetical tetrachloroethylene (PCE) spill was simulated in four sets of two-dimensional profiles extracted from these realizations. Comparisons of saturation profiles and spatial moments from point source DNAPL infiltration simulations suggest that choices involving the geostatistical algorithm used to model  $k$  and the incorporation of variable versus uniform porosity have a smaller influence than choices involving the scaling of capillary retention properties to  $k$ . From these simulations it is apparent that the degree of spatial correlation in  $P_c$ -Sat parameters exerts a controlling influence on predicted DNAPL spreading and redistribution in saturated aquifers. The resultant distribution of mass within a DNAPL source zone will have implications for DNAPL recovery and subsequent mass fluxes in remediation operations. **INDEX TERMS:** 1829 Hydrology: Groundwater hydrology; 1869 Hydrology: Stochastic processes; 1832 Hydrology: Groundwater transport; **KEYWORDS:** DNAPL entrapment, DNAPL source zone, geostatistics, heterogeneity, nonuniformity, stochastic simulation

**Citation:** Lemke, L. D., L. M. Abriola, and P. Goovaerts (2004), Dense nonaqueous phase liquid (DNAPL) source zone characterization: Influence of hydraulic property correlation on predictions of DNAPL infiltration and entrapment, *Water Resour. Res.*, 40, W01511, doi:10.1029/2003WR001980.

## 1. Introduction

[2] Many organic industrial chemicals and petroleum derivatives such as chlorinated solvents or polynuclear aromatic hydrocarbons are not readily soluble in water. Such compounds exist as separate, nonaqueous phase liquids (NAPLs). Spilled NAPLs migrating through the vadose or saturated zones under gravitational and capillary forces can become entrapped in the subsurface environment [Wilson *et al.*, 1990]. At residual organic saturation, NAPL becomes discontinuous and is immobilized by capillary forces [Mercer and Cohen, 1990]. The presence of residual NAPL ganglia

or pools within a formation is difficult to detect yet can create a persistent dissolved contaminant source, not readily amenable to effective remediation by traditional pump and treat technologies [National Research Council, 1994]. Nonuniformity and heterogeneity in soil properties contribute to spreading and irregular distributions of entrapped NAPLs [Kueper and Frind, 1991a, 1991b; Essaid and Hess, 1993; Kueper and Gerhard, 1995; Dekker and Abriola, 2000a]. In addition, the presence of low-permeability zones can inhibit uniform delivery of surfactants and subsequent advective transport of solubilized or mobilized contaminant [Fountain *et al.*, 1996; Fountain, 1997; Saenton *et al.*, 2002]. DNAPL source zone architecture [Sale and McWhorter, 2001] as well as the variance and spatial correlation of the aquifer permeability field [Dekker and Abriola, 2000b] can strongly influence remedial performance and mass flux. Representation of aquifer heterogeneities and

<sup>1</sup>Now at Department of Geology, Wayne State University, Detroit, Michigan, USA.

nonuniformities is therefore essential to the modeling of entrapped NAPL distributions necessary for the prediction of dissolved phase contaminant flux or the evaluation of alternative remediation strategies [*Strategic Environmental Research and Development Program and Environmental Security Technology Certification Program*, 2002].

[3] Numerical multiphase flow models incorporate aquifer nonuniformity through specification of the distribution of spatially variable aquifer properties including intrinsic permeability, porosity, relative permeability, and capillary pressure-saturation ( $P_c$ -Sat) relationships. A few studies have applied multiphase models to the investigation of organic liquid behavior in spatially variable systems [*Kueper and Frind*, 1991a; *Essaid and Hess*, 1993; *Kueper and Gerhard*, 1995; *Rathfelder and Abriola*, 1998; *Dekker and Abriola*, 2000a]. These investigations have revealed the substantial influence of the spatial distribution of parameters such as permeability and capillary retention on the prediction of immiscible flow pathways and organic spreading. The trend of increased spreading with increased heterogeneity observed in these numerical studies has also been observed in the field, at sites of existing spills [e.g., *Essaid et al.*, 1993] and controlled releases of dense nonaqueous phase liquids (DNAPLs) [e.g., *Kueper et al.*, 1993]. In general, a relatively small degree of horizontal bedding has been observed to result in a pronounced preferential lateral migration of organic [*Poulsen and Kueper*, 1992; *Essaid et al.*, 1993; *Kueper et al.*, 1993]. Clearly, the incorporation of spatial variability in permeability, porosity, and  $P_c$ -Sat parameters is essential for the reproduction of lateral spreading and irregular entrapped organic saturation distributions observed in laboratory and field DNAPL releases [*Kueper and Frind*, 1991b; *Essaid and Hess*, 1993]. The degree to which correlation in the spatial variability of these parameters can influence model predictions of immiscible organic contaminant infiltration and distribution, however, has not been fully explored.

[4] In the absence of exhaustive data, modeling decisions are necessary to specify the spatial distribution and relationships of aquifer characteristics. These decisions involve choices with respect to the application of deterministic or stochastic approaches used to characterize the spatial distribution of primary aquifer variables such as permeability and porosity as well as assumptions relating to the representation of spatial correlation among constitutive parameters. Understanding the implications of such choices and assumptions for the prediction of DNAPL spill behavior can contribute to the development of more realistic source zone models for use in predicting contaminant mass flux and DNAPL recovery. The objective of this paper is to investigate the influence of aquifer characterization decisions on predicted DNAPL distributions for a hypothetical spill in a saturated aquifer with nonuniform hydraulic properties. To this end, Monte Carlo simulations were employed to compute DNAPL distribution statistics for ensembles of realizations generated using four contrasting aquifer characterization approaches. Each of the four approaches incorporated aquifer property data collected at an actual field site, but differed in the selection of geostatistical simulation algorithms or the treatment of individual parameter correlation. The resulting differences in predicted source zone configuration metrics, including vertical penetration, lateral spreading, and maxi-

mum organic liquid saturations, were quantified for each ensemble so that differences among the sets could be examined herein. Variations in contaminant recovery and mass flux estimates resulting from these alternative models will be explored in a subsequent paper.

## 2. Mathematical Formulation and Numerical Implementation

[5] Modeling the simultaneous movement of two or more fluids in the subsurface entails a conceptual understanding of the interactions among fluids as well as the relationship between each fluid and the properties of the porous medium. In addition to equations governing multiphase flow, mathematical multiphase flow models incorporate constitutive equations for fluid retention and relative permeability introducing additional physical parameters. Thus a set of aquifer properties and constitutive parameters, each of which can vary spatially independently or independently of the others, must be specified across the model domain.

[6] Numerical simulations in this study were performed using M-VALOR [*Abriola et al.*, 1992; *Rathfelder and Abriola*, 1998], a two-dimensional (in a vertical cross section), block-centered, finite difference immiscible fluid flow simulator capable of incorporating nodal spatial variability in aquifer properties and constitutive parameters. M-VALOR solves a system of pressure and saturation equations using an iterative implicit pressure-explicit saturation scheme. First order upstream weighting is employed for interblock transmissibilities. The code was extended to include the Brooks-Corey-Burdine  $P_c$ -Sat and relative permeability formulations. M-VALOR has been verified against analytical solutions [*Demond et al.*, 1996] and with laboratory sandbox data for the infiltration of chlorinated solvents under heterogeneous conditions [*Rathfelder et al.*, 2003].

[7] M-VALOR solves coupled mass balance equations of the form [*Abriola et al.*, 1992]:

$$\frac{\partial}{\partial t} (\phi S_\alpha \rho_\alpha) = \nabla \cdot \left( \frac{\mathbf{k} k_{r\alpha}}{\mu_\alpha} \nabla (P_\alpha - \rho_\alpha g z) \right) + q_\alpha. \quad (1)$$

Here  $\alpha$  denotes the fluid phase ( $\alpha = w, o$  for water and organic phases, respectively, in a two phase system),  $\phi$  is the porosity,  $S_\alpha$  is the  $\alpha$ -fluid saturation,  $\rho_\alpha$  is the  $\alpha$ -fluid density,  $\mathbf{k}$  is the intrinsic permeability tensor,  $k_{r\alpha}$  is the relative permeability to the  $\alpha$ -fluid,  $g$  is gravitational acceleration,  $\mu_\alpha$  is the  $\alpha$ -fluid dynamic viscosity,  $P_\alpha$  denotes the pressure in phase  $\alpha$ , and  $q_\alpha$  is an external source/sink term.

[8] Modeling studies have indicated that hysteresis and NAPL entrapment must be included in numerical models to obtain accurate representation of two-phase immiscible liquid migration [*Essaid et al.*, 1993; *Kueper et al.*, 1993; *Van Geel and Sykes*, 1994]. Hysteresis and entrapment are incorporated into M-VALOR using the parametric model of *Kaluarachchi and Parker* [1992]. The approach utilizes the *Land* [1968] equation to calculate the effective residual organic phase along any imbibition scanning curve:

$$\bar{S}_{or} = \frac{1 - \bar{S}_w^{\min}}{1 + R \left( 1 - \bar{S}_w^{\min} \right)}, \quad \text{where } R = \frac{1 - S_{wr}}{S_{or}^{\max}} - 1. \quad (2)$$

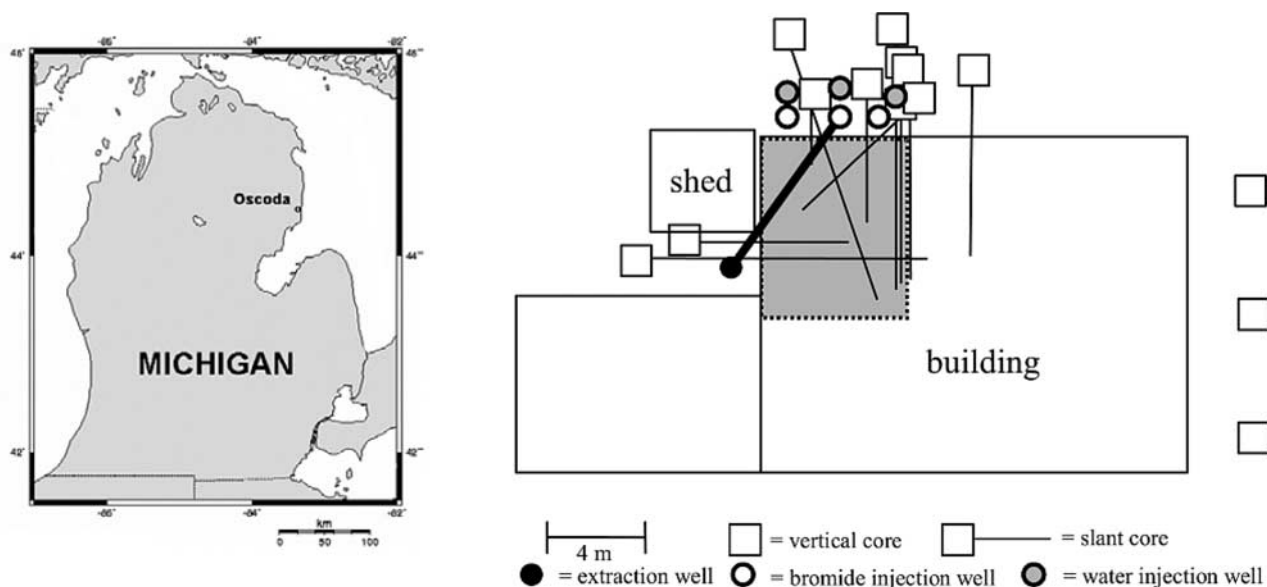


**Figure 1.** Location of the field study site in Oscoda, Michigan. The position of vertical and oriented soil cores is shown. The suspected PCE source zone targeted in the SEAR pilot test is shaded. The thick SW-NE line indicates the position of two-dimensional vertical profiles extracted from three-dimensional geostatistical simulations.

Here  $\bar{S}_w^{\min}$  is the minimum effective water saturation prior to imbibition,  $S_{wr}$  is the residual or irreducible water saturation, and  $S_{or}^{\max}$  is the residual organic phase saturation defined by the main imbibition curve. An apparent effective water saturation,  $\bar{S}_w$ , is defined by:

$$\bar{S}_w = \bar{S}_w + \bar{S}_{ot}, \quad (3)$$

where  $\bar{S}_w$  is the effective water saturation  $((S_w - S_{wr}) / (1 - S_{wr}))$ , and  $\bar{S}_{ot}$  is the normalized trapped or immobile organic phase saturation [Parker and Lenhard, 1987]. For any point along a scanning imbibition curve originating at  $\bar{S}_w^{\min}$  on the primary drainage curve, the quantity of entrapped organic between  $\bar{S}_{ot} = 0$  at  $\bar{S}_w = \bar{S}_w^{\min}$  and  $\bar{S}_{ot} = \bar{S}_{or}$  at  $\bar{S}_w = 1$  is estimated by linear interpolation [Parker and Lenhard, 1987]:

$$\bar{S}_{ot} = \bar{S}_{or} \left( \frac{\bar{S}_w - \bar{S}_w^{\min}}{(1 - \bar{S}_{or}) - \bar{S}_w^{\min}} \right). \quad (4)$$

[9] Numerical simulations in this study used the Brooks-Corey [Brooks and Corey, 1964] P<sub>c</sub>-Sat model for primary drainage:

$$\bar{S}_w = \left( \frac{P_c}{P_b} \right)^\lambda \quad \text{if } P_c \geq P_b \quad (5)$$

$$\bar{S}_w = 1.0 \quad \text{if } P_c < P_b, \quad (6)$$

where  $\lambda$  is the pore size distribution index,  $P_c$  is the capillary pressure ( $P_o - P_w$ ), and  $P_b$  is the entry or bubbling pressure. In addition, Brooks and Corey [1964] relative permeability functions, based on extensions of the work of Burdine [1953], were adopted. Closed form solutions for

these relationships are given by [Demond et al., 1996; Chen et al., 1999]:

$$k_{rw} = \bar{S}_w^{\frac{2+3\lambda}{\lambda}} \quad (7)$$

$$k_{ro} = \left(1 - \bar{S}_w\right)^2 \left(1 - \frac{\bar{S}_w^{\frac{2+\lambda}{\lambda}}}{\bar{S}_w}\right). \quad (8)$$

Hysteresis due to nonwetting phase entrapment is incorporated through the inclusion of apparent water saturations in equation (8), consistent with the observation that wetting phase relative permeability is generally a function of saturation while nonwetting phase relative permeability shows hysteresis [Demond and Roberts, 1987; Lenhard et al., 1991].

[10] Equation (1) together with the continuity equation:

$$S_w + S_o = 1.0 \quad (9)$$

and a combination of the constitutive relations for capillary pressure-saturation and relative permeability form a complete set of relationships required to model two-phase immiscible flow. For the formulation implemented in this study, a total of 10 fluid properties, aquifer properties, and constitutive parameters must be specified for these equations:  $\mu_\alpha$  and  $\rho_\alpha$  for each phase,  $\phi$ ,  $k$ ,  $S_{or}^{\max}$ ,  $S_{wr}$ , and Brooks-Corey capillary-saturation parameters  $\lambda$  and  $P_b$ .

### 3. Aquifer and DNAPL Source Zone Characterization

[11] The aquifer chosen to provide a basis for alternative characterization models used in this study is located in Oscoda, Michigan, USA, at the site of a former dry cleaning business (Figure 1) facing Bachman Road. A suspected DNAPL source zone was identified beneath the building in

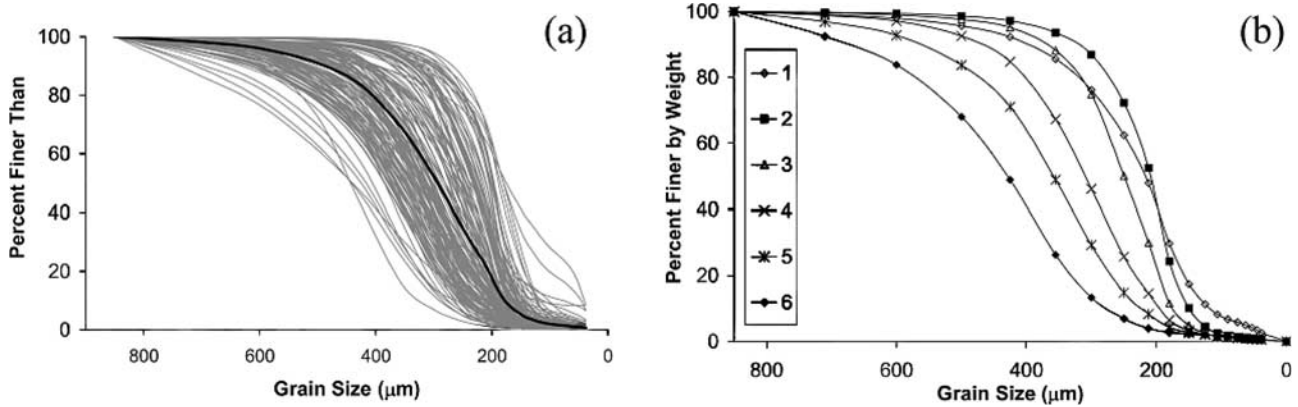


**Figure 2.** Grain size cumulative distribution function (cdf) plots: (a) Normalized distributions for 167 measured sand samples; dark line represents the 167 sample average. (b) Weighted average grain size distribution cdfs for six soil classes identified based on KMEANS clustering of normalized cdfs.

an unconfined aquifer where a narrow tetrachloroethylene (PCE) plume emanates and discharges into Lake Huron approximately 200 m down gradient [Drummond *et al.*, 2000]. The aquifer is composed of relatively homogeneous glacial outwash sands and is underlain by a thick clay layer approximately 8 m below the ground surface. A pilot-scale Surfactant Enhanced Aquifer Remediation (SEAR) test, designed to solubilize and recover residual PCE from the suspected DNAPL source zone under the building was conducted in the summer of 2000. The pilot-scale test was designed with a single extraction well, a row of three water injection wells to establish a flow field through the source zone perpendicular to the natural gradient, and a row of three surfactant injection wells positioned between the water supply and extraction wells (Figure 1) [Drummond *et al.*, 2000].

[12] Aquifer characterization efforts associated with the pilot SEAR test included analysis of 167 samples collected from 12 vertical and directional cores (Figure 1). Care was taken to avoid combining distinctly different soil textures when separating the core samples into 15 and 30 cm lengths so that macroscopic breaks (i.e., bedding) would not be obfuscated. Each sample was dried, disaggregated, and sieved to quantify grain size distributions (GSDs). GSDs were normalized to a maximum particle size of 850  $\mu\text{m}$  to reduce the influence of a multimodal gravel fraction present in about 10% of the samples (Figure 2). Such gravel size pebbles were not observed to constitute a separate layer or lag in any of the core samples. Rather they were distributed within a predominantly sand matrix. The normalization step was therefore adopted to facilitate the use of GSDs for the estimation of hydraulic conductivity and capillary retention properties judged to be controlled by the finer sediment fractions [Koltermann and Gorelick, 1995]. The arithmetic mean porosity value, measured in a subset of 162 repacked samples, was 0.36 (Figure 3). In addition, hydraulic conductivity,  $K$ , was measured for 10 repacked samples using a constant head permeameter. Isotropic  $K$  values for all samples were estimated from normalized grain size distributions using the Kozeny-Carman (K-C) equation [Bear, 1972]:

$$K = \frac{\rho_w g}{\mu_w} k = \frac{\rho_w g}{\mu_w} \left[ \frac{d_m^2}{180} \frac{\phi^3}{(1-\phi)^2} \right], \quad (10)$$

where  $d_m$  is a representative grain size. Constant fluid density and viscosity for water at 15°C were assumed, making values of  $k$  and  $K$  directly scaleable. Good agreement between measured and estimated  $K$  values (Figure 4) was achieved assuming a porosity value of 0.36 and using the normalized  $d_{10}$  value as the representative grain size. Although continuous core samples collected from the site contain relatively homogeneous fine- to medium-grained sand, estimated  $K$  values were nonuniform, ranging from 1 to 48 m/d. The variance of the lognormal transformation of the estimated  $K$  population ( $\sigma^2 \ln(K)$ ), 0.29, is similar to the values of 0.24 and 0.37 reported by Woodbury and Sudicky [1991] for  $K$  measurements made along two profiles in sandy glaciofluvial deposits at the Canadian Forces Base Borden, Ontario, and to the value of 0.24 reported by Hess *et al.* [1991] for a sand and gravel glacial outwash deposit on Cape Cod, Massachusetts.

[13] Six individual soil classes were identified based on KMEANS clustering of the 167 measured grain size distributions following the approach of Schad [1993] (Figure 2). Air-water  $P_c$ -Sat curves (Figure 5) were measured for samples from each of the six soil classes using a pressure cell apparatus developed by Salehzadeh and Demond [1999]. Retention curves estimated from grain size distribution curves and porosity values using the Haverkamp and Parlange [1986] method compared favorably with the measured curves (Figure 5).

[14] In support of the pilot SEAR test, three-dimensional, nonuniform  $\phi$  and  $K$  distributions were generated using geostatistics over a  $30 \times 30 \times 10$  m grid centered on the suspected DNAPL source zone. The domain was large enough to encompass all core sampling points which were used as conditioning data. Grid discretization of 30 cm for geostatistical modeling corresponded directly to the scale of support for core sample data used to measure or estimate  $\phi$  and  $K$ . Infiltration and entrapment of PCE was modeled along two-dimensional vertical profiles extracted from the three-dimensional geostatistical realizations. The use of two-dimensional profiles permitted the application of Monte Carlo analysis to evaluate variability among ensembles of realizations. Numerical PCE infiltration experiments were run on a set of Sun Microsystems Ultra 1, Ultra 5, and Ultra 10 workstations. The average CPU time for each of this investigation's 200 simulations was 5.3 hours. Each profile

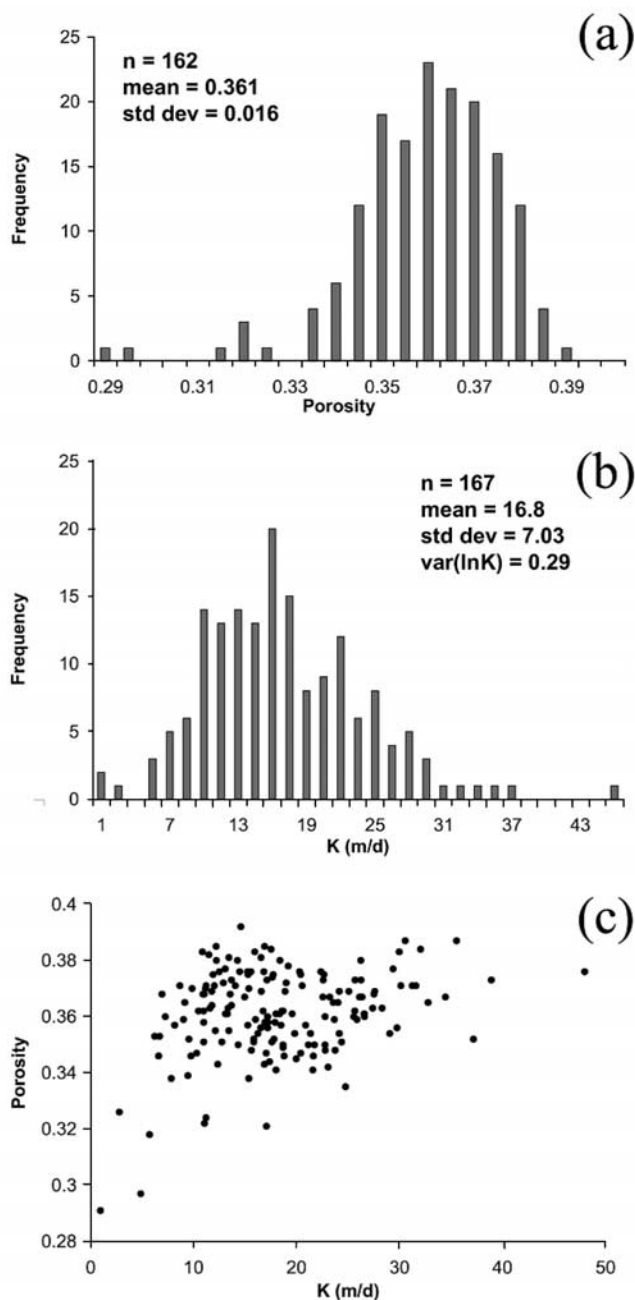


**Figure 3.** Porosity and hydraulic conductivity data: (a) Histogram of measured porosity values for repacked samples. (b) Histogram of  $K$  values estimated directly from measured grain size distribution  $d_{10}$  values using the Kozeny-Carman relationship (equation (10)) with a uniform porosity of 0.36. (c) Cross plot of  $\phi$  and  $K$  values for 162 core samples. Scatter on this plot suggests a weak correlation between variables. The  $R^2$  value for a linear regression is 0.09.

is oriented SW-NE along a 7.65 m flow path passing through the suspected DNAPL source zone and connecting the SEAR extraction and middle surfactant injection wells (Figure 1). The position of these profiles was chosen in anticipation of simulations designed to model DNAPL recovery and effluent mass flux under natural gradient and enhanced recovery conditions similar to those found at the Bachman site.

[15] Prior to the pilot-scale SEAR test, the distribution and volume of entrapped PCE at the Bachman Road site was unknown. At some spatial sampling points beneath the building, aqueous phase concentrations approached the PCE solubility limit [Drummond *et al.*, 2000] and visible staining was observed along floor joists beneath a portion of the building, suggesting that the likely source of PCE was spills and leaks that infiltrated the earthen floor of the crawl space above the suspected source zone. Because no significant free phase PCE was detected during coring and aquifer fluid sampling, the majority of DNAPL was thought to be in the form of entrapped residual. A PCE spill scenario consisting of small volumes of solvent released over long periods of time is consistent with the suspected spill history at the Bachman site.

## 4. Methods

### 4.1. Alternative Geostatistical Simulation Approaches

[16] The application of stochastic modeling to flow and transport problems has become increasingly widespread over the last three decades and a wide variety of geostatistical simulation algorithms have been developed to address flow and transport variables as spatially random functions [Meyers, 1997; Goovaerts, 1999]. Stochastic simulation methods can generate multiple, equally probable realizations of nonuniform or heterogeneous aquifer properties, each honoring the properties' statistical spatial structure and probability distribution [Srivastava, 1994]. Two of the most common methods, sequential Gaussian simulation (SGS) and sequential indicator simulation (SIS) [Deutsch and Journel, 1998], were employed in this study to generate three-dimensional, nonuniform  $\phi$  and  $K$  fields.

[17] SGS relies on an analytical model for the random function distribution. It assumes that the random function multivariate distribution (or commonly its natural logarithm) is Gaussian so that the univariate distribution can be completely characterized by two parameters, the mean and variance, and the bivariate (two-point) distribution requires only the covariance or semivariogram as additional information. If an original sample histogram is not normal,

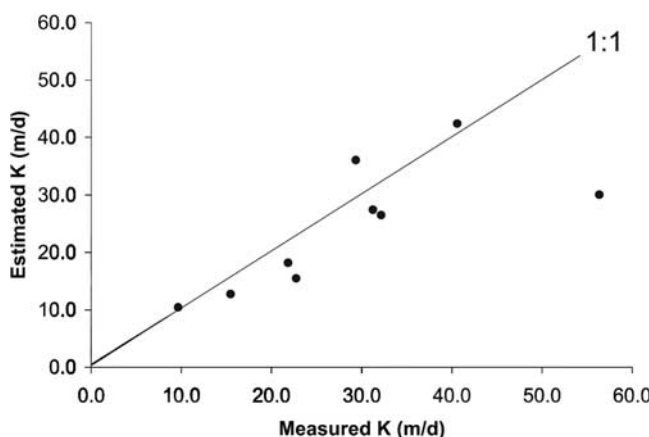


**Figure 4.** Comparison of laboratory-measured and estimated  $K$  values. Estimates were obtained from the Kozeny-Carman relationship (equation (10)) assuming 0.36 porosity and using the normalized  $d_{10}$  value as the representative grain size.

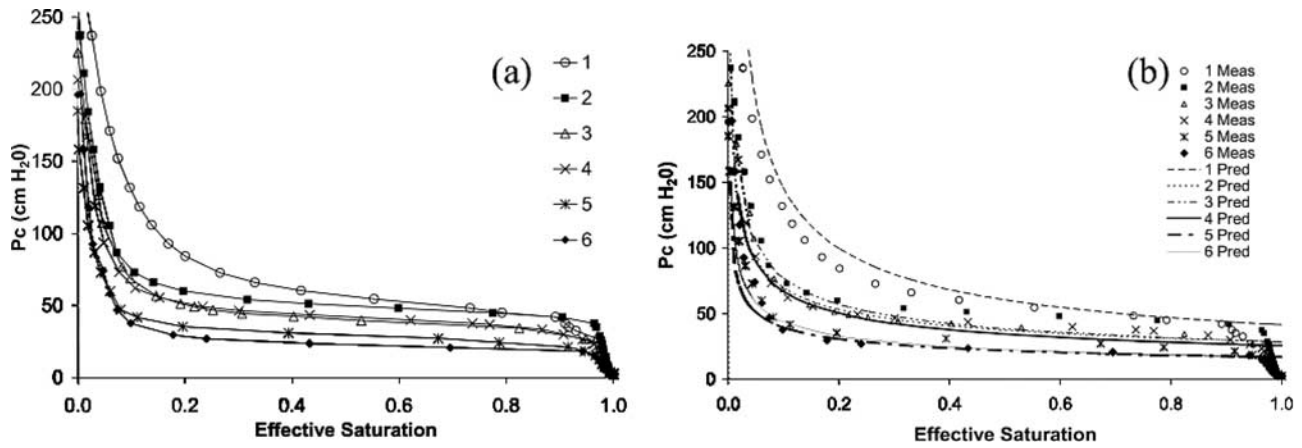


**Figure 5.** Capillary pressure-saturation curves: (a) Laboratory-measured air-water  $P_c$ -Sat curves for samples from each of the six soil classes identified in Figure 2b. (b) Comparison of laboratory-measured and predicted  $P_c$ -Sat curves. Predicted retention curves are estimated from grain size distribution curves and porosity values using the *Haverkamp and Parlange* [1986] method.

the log or normal score transform can be used prior to simulation followed by a back transform of the simulated values [Deutsch and Journel, 1998]. Conversely, in SIS no assumption is made about the shape of the random function distribution, which, consequently, can be used to characterize the spatial variability of categorical (i.e., discrete valued random functions) as well as continuous variables.

[18] In sequential simulation, a random path is followed to visit each unsimulated grid node. For SGS, multi-Gaussian kriging is used to estimate the local cumulative distribution function (cdf) at each node, conditioned to all known and previously simulated data points, by assuming that it is Gaussian. The attribute value assigned to the grid node is then drawn at random from the local conditional cumulative distribution function (ccdf) [Srivastava, 1994]. The process is repeated until all unsimulated grid nodes have been visited. Sequential simulation requires a kriging system solution for every node [Deutsch and Journel, 1998] which makes it computationally demanding. The major drawback associated with SGS, however, may be its inability to preserve the occurrence of continuous units that can be critical to flow and transport because of its tendency to maximize the entropy associated with the simulation [Journel and Deutsch, 1993; Gomez-Hernandez, 1997; Gomez-Hernandez and Wen, 1998].

[19] SIS relies on indicator coding of data, which model the probability that the value of an attribute  $z_k$ , at an unsampled location,  $\mathbf{u}_\alpha$ , is no greater than a given threshold:

$$i(\mathbf{u}_\alpha; z_k) = \begin{cases} 1 & \text{if } z(\mathbf{u}_\alpha) \leq z_k \\ 0 & \text{if } z(\mathbf{u}_\alpha) > z_k \end{cases} \quad (11)$$

Here  $i(\mathbf{u}_\alpha; z_k)$  is the indicator value at location  $\mathbf{u}_\alpha$  defined with respect to the threshold value  $z_k$ . Continuous variables are thus discretized using a set of  $n = 1, 2, \dots, N$  threshold values. Alternatively, threshold values can represent a set of  $N$  discrete categories. In this case, the indicator coding corresponds to the presence or absence of the category rather than indicating whether a threshold value has been exceeded [Goovaerts, 1997, 1998]. Semivariograms are modeled as a continuous function of the separation vector

between points using a linear combination of permissible (positive semi-definite) variogram models for each indicator class. SIS follows the same procedure as SGS, assigning values to each node in the domain in random order, except that indicator kriging is used to model the local ccdf at each point. However, because SIS does not assume a particular distribution for the random function, it has several advantages over Gaussian algorithms. As discussed above, it can be applied to continuous variables or mutually exclusive classes of soil types. Indicator simulation has the potential to reproduce spatial correlation of extremely large or small values [Goovaerts, 1997] that may be important for replicating continuity in preferential flow paths or barriers within pixel-based simulations. Furthermore, like other nonparametric stochastic simulation algorithms, SIS generally provides more flexibility to incorporate soft geological and geophysical information [Koltermann and Gorelick, 1996].

[20] Because of their ability to represent categorical data, indicator statistics are commonly employed to simulate the distribution of aquifer or reservoir facies with distinct or heterogeneous property distributions [e.g., Johnson and Dreiss, 1989; Poeter and Townsend, 1990; Rubin and Journel, 1991; Goggin and Jordan, 1995; Johnson, 1995; Ritzi et al., 1995; Dominic et al., 1998]. Fewer studies have employed indicator statistics to model categories within a single facies [e.g., Schad, 1993; Ptak, 1997]. In the present study, the data are treated as nonuniform, but statistically homogeneous, rather than heterogeneous. For a useful discussion of the distinction between the terms nonuniformity and heterogeneity, the interested reader is referred to Greenkorn and Kessler [1969] and Freeze [1975]. This treatment, combined with the use of SIS, results in preservation of continuity of low and high indicator class values. Note that the transformation of indicator values to aquifer parameters (i.e.,  $d_{10}$  values) can impart an additional random component that diminishes spatial continuity of high and low values when modeling nonuniform rather than heterogeneous distributions.

#### 4.2. Spatial Variability of $\phi$ and $K$

[21] Porosity measurements and hydraulic conductivity estimates are poorly correlated at the Bachman Road site, as

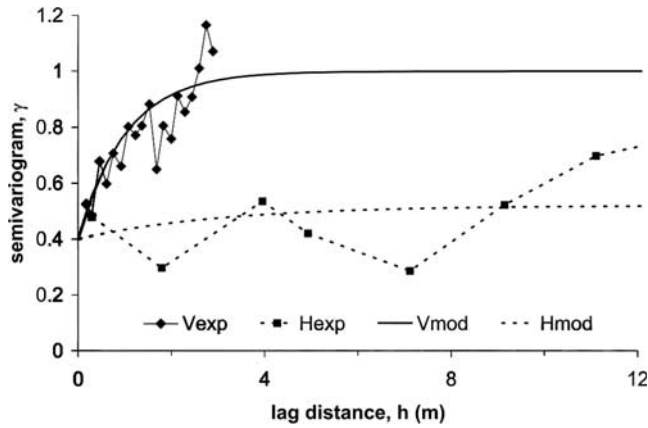


**Figure 6.** Experimental and modeled normal score semivariograms for measured porosity data. The plot is normalized to the variance to generate a sill of 1.0. Vexp is vertical experimental; Hexp is horizontal experimental; Vmod is vertical modeled; Hmod is horizontal modeled.

illustrated by the  $\phi$ - $K$  cross plot (Figure 3). Therefore  $\phi$  and  $K$  were simulated independently. Although nonuniform in their distribution, both  $\phi$  and  $K$  were judged to be statistically homogeneous. That is, the data are believed to be taken from a single depositional unit and can be pooled across the study area for the purpose of inferring random function cdfs and moments. Second order stationarity is herein adopted so that the expected value of the random function is constant and the covariance between two random variables at  $\mathbf{u}$  and  $\mathbf{u} + \mathbf{h}$  does not depend on the location  $\mathbf{u}$ , but only upon the separation vector,  $\mathbf{h}$  [Goovaerts, 1997]. Analysis of variance and geostatistical simulation were conducted in three-dimensions to maximize the number of data pairs used to define experimental variograms and to incorporate all available data as conditioning points within each geostatistical realization.

[22] Two approaches were used to model porosity. In the first, a uniform porosity equivalent to the arithmetic mean of the measured porosity values was assumed. In the second, SGS was used to create multiple nonuniform realizations conditioned to the 162 sample points with measured porosity values. The latter approach required a prior normalization of the sample probability distribution. Experimental vertical and horizontal semivariograms for normal score transforms of porosity measurements (Figure 6) were fit with a zonal anisotropy model [Journel and Huijbregts, 1978] including a nugget effect of 0.4 estimated from the vertical semivariogram and an exponential semivariogram model:

$$\gamma(h) = c \cdot \left[ 1.0 - \exp\left(-\frac{3h}{a}\right) \right], \quad (12)$$

where  $\gamma(h)$  is the semivariogram value for a lag distance  $h$ ,  $c$  is a positive contribution to the variance, and  $a$  is the direction-dependent range, which is equivalent to three times the integral scale. Variability in the horizontal plane was modeled as isotropic. Variogram model parameters used in geostatistical simulations are given in Table 1.

[23] Three-dimensional, nonuniform  $K$  fields, conditioned at the 167 core sample points across the study area, were

**Table 1.** Variogram Parameters for SGS Geostatistical Modeling of Porosity and Representative Grain Diameter

Model	Orientation	Nugget <sup>a</sup>	Variance <sup>a,b</sup>	Range, m	Integral Scale, m
SGS $\phi$	Horizontal	0.40	0.52	9.14	3.05
SGS $\phi$	Vertical	0.40	1.00	3.05	1.02
SGS $d_{10}$	Horizontal	0.333	0.80	7.00	2.33
SGS $d_{10}$	Vertical	0.333	1.00	1.07	0.36

<sup>a</sup>Variance normalized to 1.0.

<sup>b</sup>Includes nugget effect contribution.

simulated using two alternative geostatistical approaches. Initially, SGS was used to simulate conditional  $d_{10}$  grain size values that were subsequently converted to  $K$  values using the Kozeny-Carman relationship (equation (10)). Experimental semivariograms for  $d_{10}$  values (Figure 7) were fit with a zonal anisotropy model including a nugget effect of 0.333 estimated from the vertical semivariogram and a spherical semivariogram model:

$$\gamma(h) = c \cdot \left[ 1.5 \left( \frac{h}{a} \right) - 0.5 \left( \frac{h}{a} \right)^3 \right] \quad \text{if } h \leq a \quad (13)$$

$$\gamma(h) = c \quad \text{if } h \geq a, \quad (14)$$

where  $\gamma(h)$  is the semivariogram value for a lag distance,  $h$ ,  $c$  is a positive contribution to the variance, and  $a$  is the direction-dependent range (Table 1). Variability in the horizontal plane was modeled as isotropic.

[24] The second modeling approach was implemented using a three step procedure to generate conditional  $K$  field realizations using SIS: (1) simulation of the spatial distribution of six indicator classes representing categories of grain size distributions (indicator class variogram parameters are given in Table 2); (2) random assignment of  $d_{10}$  values to each grid node based upon smoothed  $d_{10}$  value histograms for each indicator class (Figure 8); and (3)  $K$  value calculation using equation (10) assuming uniform or stochastically simulated porosity fields.

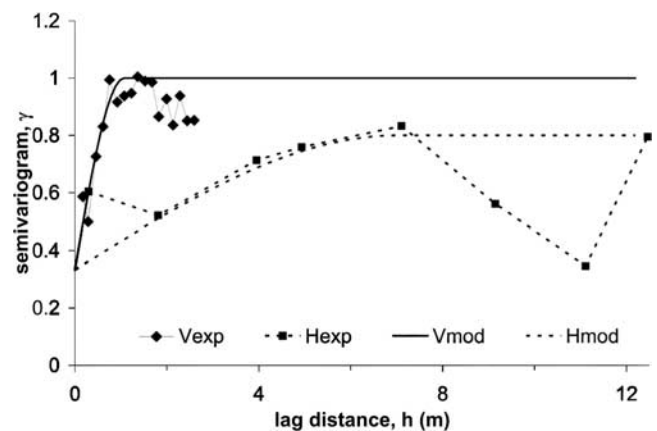


**Figure 7.** Experimental and modeled normal score semivariograms for measured grain size distribution  $d_{10}$  data. The plot is normalized to the variance to generate a sill of 1.0. A zonal anisotropy model is employed.

**Table 2.** Variogram Parameters for SIS Geostatistical Modeling

Indicator Class <sup>a</sup>	Orientation	Nugget	Variance <sup>b</sup>	Range a, m	Integral Scale, m	Global, %
1	horizontal	0.00	0.012	3.05	1.02	1.0
1	vertical	0.00	0.012	0.003	.001	
2	horizontal	0.02	0.070	2.74	0.91	13.0
2	vertical	0.02	0.075	0.49	0.16	
3	horizontal	0.15	0.165	0.91	0.30	23.0
3	vertical	0.15	0.205	0.70	0.23	
4	horizontal	0.13	0.060	1.83	0.61	27.0
4	vertical	0.13	0.060	0.91	0.30	
5	horizontal	0.13	0.180	3.66	1.22	32.0
5	vertical	0.13	0.260	1.28	0.43	
6	horizontal	.005	0.052	7.32	2.44	4.0
6	vertical	.005	0.052	0.88	0.29	

<sup>a</sup>Indicator classes are based on the six soil classes presented in Figure 2b.

<sup>b</sup>Includes nugget effect contribution.

[25] Horizontal and vertical  $\phi$ ,  $d_{10}$  and indicator variograms (Figures 6 and 7) support a zonal anisotropy model typical of stratified media with greater variability in the vertical direction [Kupfersberger and Deutsch, 1999]. A uniform  $K_v/K_h$  ratio of 0.5 was assigned to all  $K$  values to account for anisotropy related to aquifer stratification at a scale finer than that resolved by the geostatistical models.

#### 4.3. Spatial Variability of Additional Aquifer Parameters

[26] Capillary pressure-saturation parameters may also vary spatially. Direct laboratory measurement of these properties from field samples is expensive and time consuming for large sample sets. Consequently, for unconsolidated sandy aquifers, empirical methods are frequently used to estimate retention curves from grain size distribution measurements [Arya and Paris, 1981; Haverkamp and Parlange, 1986; Arya and Dierolf, 1992]. For primary drainage, both the Brooks-Corey pore size distribution factor,  $\lambda$ , and the air entry pressure,  $P_b$ , can be estimated directly from grain size distribution curves for given porosity and dry bulk density values using the Haverkamp and Parlange [1986] method (HPM). The HPM estimates  $\lambda$  as a function of porosity, bulk density, and two fitting parameters derived from matching a van Genuchten-type

functional form to the particle size distribution curve.  $P_b$  is then obtained through the iterative solution of a relationship between  $\lambda$ ,  $\phi$ , and an empirically derived packing coefficient. Air entry pressures thus obtained can be scaled to organic liquid-water systems using a ratio of interfacial tensions.

[27] Utilization of the Haverkamp and Parlange method provides two alternatives for the assignment of spatially variable  $P_c$ -Sat parameters. The traditional approach, commonly referred to as Leverett scaling, scales the entry pressure for a representative retention curve,  $P_c^{ref}$ , using a ratio of intrinsic permeability and porosity values [Leverett, 1941]:

$$P'_c = P_c^{ref} \sqrt{\frac{k^{ref} \phi'}{k' \phi^{ref}}} \quad (15)$$

In this approach, the pore size distribution factor is not scaled so that the  $P_c$ -Sat curve is translated up or down with respect to capillary pressure while its shape does not change. If uniform porosity is assumed, the representative retention curve is simply scaled to  $k$  at each node of the geostatistical realization. A consequence of this method is the adoption of completely correlated  $k$  and  $P_c$ -Sat distributions. An alternative to Leverett scaling is possible in conjunction with sequential indicator simulation of categorical values defined using grain size distribution patterns. In this approach, the HPM is used to derive values for  $P_b$  and  $\lambda$  using the representative grain size distribution curve associated with the simulated indicator class at each node. Nodal porosity and bulk density values can also be used if they vary in space. A consequence of this approach is a decrease in the dependency between  $P_b$  and  $k$  values. Differences in multiphase flow model behavior arising from alternative approaches to parameter distribution correlation are not well understood, however, and systematic evaluations of the consequences of simplifying assumptions such as uniform porosity and retention curve scaling have not been well documented in the literature.

[28] In this study, water is considered the wetting phase while organic liquids are considered nonwetting fluids. Dekker and Abriola [2000a] reported that correlation

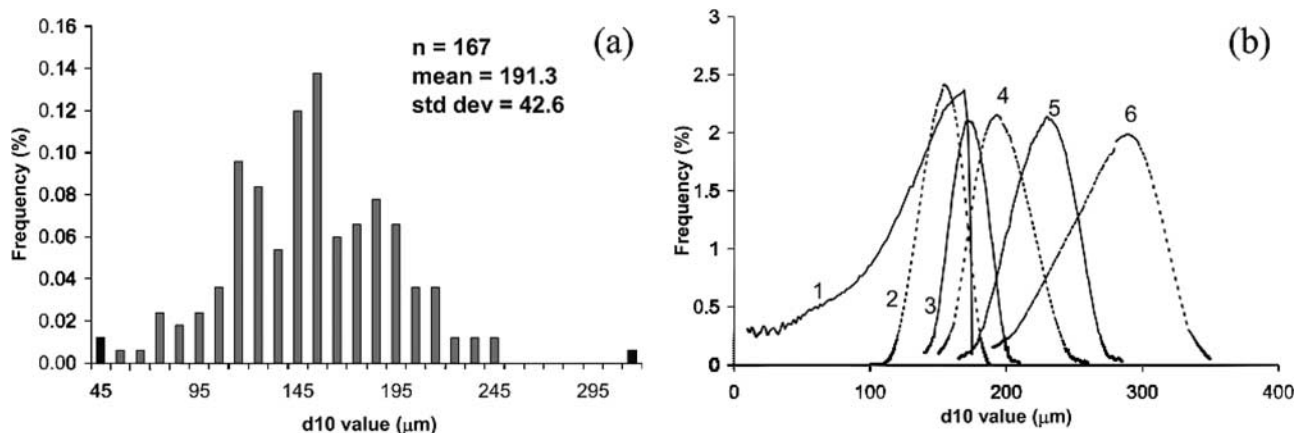


**Figure 8.** Grain size distribution  $d_{10}$  values: (a) probability distribution function (pdf) of  $d_{10}$  values and (b) smoothed  $d_{10}$  pdfs for six individual indicator classes. Global frequency of occurrence for each indicator class is given in Table 2.

**Table 3.** Variable Treatment of Porosity, Intrinsic Permeability, and Brooks-Corey Capillary Pressure-Saturation Parameters Among the Four Alternative Simulation Sets

	Reference Set	Set 1	Set 2	Set 3
Porosity, $\phi$	uniform	uniform	random (SGS)	random (SGS)
Permeability, $k$	SGS $k = f(d_{10})$	SIS $k = f(d_{10})$	SIS $k = f(d_{10}, \phi)$	SIS $k = f(d_{10}, \phi)$
Brooks-Corey $P_c$ -Sat	weighted average $P_b$ and $\lambda$	weighted average $P_b$ and $\lambda$	weighted average $P_b$ and $\lambda$	separate $P_b$ and $\lambda$ by IC and $\phi$
Leverett Scaling	$P_b$ scaled by $\sqrt{k}$	$P_b$ scaled by $\sqrt{k}$	$P_b$ scaled by $\sqrt{k, \phi}$	none: $P_b = f(IC, \phi)$

between residual water saturation and the permeability field had statistically insignificant effects on simulated PCE spill behavior in a saturated sand aquifer. A similar lack of influence was reported for cross correlation between residual organic liquid saturation and  $k$  within the limits of experimental observations [Dekker and Abriola, 2000a]. Consequently, soil parameters  $S_{wr}$  and  $S_{or}^{\max}$  are treated herein as spatially uniform. The relationship between variability in parameters  $\lambda$ , and  $P_b$  with variability in aquifer properties  $\phi$ , and  $k$  is the primary focus of this investigation.

#### 4.4. Geostatistical Ensemble Sets

[29] Four ensemble sets of 50 aquifer realizations were generated to investigate the influence of aquifer characterization decisions on predicted multiphase flow and entrapment behavior. DNAPL infiltration simulation results were analyzed for an increasing number of realizations in each set until the mean value for each of the model performance metrics described in section 4.6 stabilized [Lemke, 2003]. The first ensemble, termed the reference set, assumed a uniform average porosity of 0.36 and utilized SGS to simulate three-dimensional distributions of  $d_{10}$  values. Hydraulic conductivity values were then calculated as a function of the uniform porosity and simulated  $d_{10}$  values at each node using equation (10). A single, representative  $P_c$ -Sat curve was estimated using HPM based on a weighted average GSD curve calculated from the 167 individual GSD curves (Figure 2a). The  $\lambda$  value from the representative curve was assigned uniformly to all nodes, consistent with the similar shapes of grain size distributions for indicator classes 2–6 in Figure 2b. The representative  $P_b$  value was scaled according to the simulated permeability at each node (equation (15)). This approach is similar to that used by Kueper and Frind [1991b], Kueper and Gerhard [1995], and Dekker and Abriola [2000a], who generated Gaussian spatially-correlated random permeability fields, assumed constant porosity, and scaled capillary pressure-saturation curves to  $k$  using modified Leverett scaling.

[30] Three additional simulation sets (sets 1, 2, and 3) were created to explore differences in predicted DNAPL distributions related to variability in porosity, permeability, and Brooks-Corey  $P_c$ -Sat parameter distributions (Table 3). Set 1 realizations are identical to the reference set except that the spatial distribution of  $d_{10}$  values was generated in two steps: (1) the spatial distribution of six categories of grain size distributions was simulated using SIS, and (2)  $d_{10}$  values were assigned randomly from histograms corresponding to each of the six indicator classes (Figure 8).

[31] Set 2 realizations differ from set 1 in that porosity was simulated as an independent random field using SGS. Hydraulic conductivity and permeability values were then

calculated as a function of both the simulated porosity and  $d_{10}$  values at each grid node.

[32] Simulation sets 2 and 3 share identical porosity and permeability distributions but differ in the assignment of capillary pressure parameters. Set 2 employs Leverett scaling to scale a representative  $P_b$  value to  $k$  and  $\phi$  at each simulation node. In set 3, individual  $P_b$  and  $\lambda$  values were assigned based on HPM calculations using the simulated porosity value and the grain size distribution corresponding to the simulated class (Figure 9) at each node. Leverett scaling of  $P_b$  values was not applied.

#### 4.5. Simulated DNAPL Release

[33] The infiltration and entrapment of a hypothetical PCE spill were modeled in two-dimensional profiles extracted from the three-dimensional geostatistical realizations described above. In each M-VALOR run, 96 liters of PCE was released over four cells located at the top center of the model, at a constant flux of 240 ml/day for 400 days. An additional 330 days was simulated to allow for subsequent organic liquid infiltration and redistribution. Constant pressure and saturation boundaries were maintained along the profile sides and a no-flow boundary was imposed at the base of the model domain. Preliminary simulations confirmed that a 96 liter PCE release produced organic liquid distributions that were spread vertically and horizontally throughout a large portion of the model domain but did not result in basal pooling or PCE migration across lateral profile boundaries. This behavior

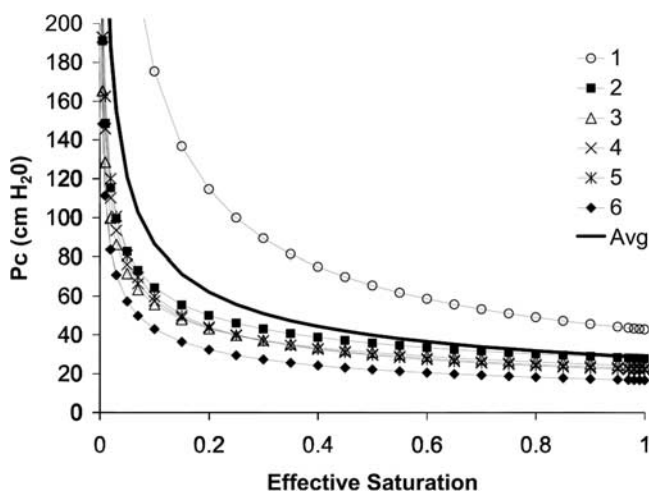


**Figure 9.** Weighted average  $P_c$ -Sat curves for each indicator class estimated using the Haverkamp and Parlange method assuming a porosity of 0.36. A single weighted average curve for the entire sample population is shown as a thick solid line.

**Table 4.** M-VALOR Simulation Input Parameters

Variable	Water	PCE
Density (kg/m <sup>3</sup> )	999.032	1623.0
Viscosity (kg/m s)	$1.139 \times 10^{-3}$	$8.900 \times 10^{-4}$
Compressibility (Pa <sup>-1</sup> )	$4.4 \times 10^{-10}$	0.0
$S_{wr}$	0.08	
$S_{or}$	0.151	
$\sigma_{a/w}$ (d/cm)	72.0	
$\sigma_{a/o}$ (d/cm)	31.7	
$\sigma_{o/w}$ (d/cm)	47.8	

was desirable to insure consistent total PCE mass in all realizations while maximizing the area contacted by organic liquid so that organic liquid distributions were influenced by spatial variability over a representative portion of the model domain. Table 4 contains a list of M-VALOR simulation input parameters.

[34] Sensitivity to horizontal and vertical grid refinement was explored using both the *Brooks and Corey* [1964] and *van Genuchten* [1980]  $P_c$ -Sat formulations following the approach of *Rathfelder and Abriola* [1998]. Simulations utilizing the van Genuchten approach demonstrated convergence in spreading behavior and maximum predicted organic liquid saturations when horizontal and vertical grid increments were reduced to 30.48 cm and 7.62 cm or less, respectively. Consistent with *Rathfelder and Abriola's* [1998] results, simulations with the Brooks-Corey  $P_c$ -Sat formulation continued to display increased spreading with finer grid intervals in the vertical dimension. Maximum organic liquid saturation values were stable, however. For reasons of computational efficiency resulting from the large number of simulations required for Monte Carlo analysis in this study, horizontal and vertical grid refinement was limited to 30.48 cm and 7.62 cm, respectively.

#### 4.6. Model Metrics

[35] Spatial moments and saturation probability distribution functions of DNAPL distributions predicted by M-VALOR simulations were analyzed to explore similarities and differences in model behavior for each ensemble set of realizations. Metrics included first and second moments and the average and maximum PCE saturation. Spatial moments were defined following *Kueper and Frind* [1991b] and *Essaid and Hess* [1993] using:

$$M_{ij} = \int_{-\infty}^{\infty} \int_{-\infty}^{\infty} \phi_{p_o} S_o(x, z) x^i z^j dx dz. \quad (16)$$

$M_{00}$ , the zeroth moment, is equivalent to the summation of PCE mass in the profile. The horizontal and vertical positions for the PCE spill center of mass are given by:

$$x_{cm} = \frac{M_{10}}{M_{00}} \quad \text{and} \quad z_{cm} = \frac{M_{01}}{M_{00}}. \quad (17)$$

The second spatial moments about the center of mass in the  $x$  and  $z$  directions, given by:

$$\sigma_{xx}^2 = \frac{M_{20}}{M_{00}} - x_{cm}^2 \quad \text{and} \quad \sigma_{zz}^2 = \frac{M_{02}}{M_{00}} - z_{cm}^2, \quad (18)$$

are a measure of horizontal and vertical organic liquid spreading, respectively.

## 5. Results

### 5.1. Aquifer Parameter Distributions

[36] Figure 10 depicts aquifer property distributions for representative profiles from each of the four simulation sets. Here, profiles with simulated PCE saturation distribution statistics (section 5.2) most closely approaching the mean ensemble value for each set were selected as representative. Simulated porosity distributions for sets 2 and 3 exhibit a strong random component due to the large nugget effect (0.40). Nevertheless, stratification in the porosity profiles is evidenced by a higher degree of continuity in high and low  $\phi$  values in the horizontal versus the vertical direction.

[37] Although a high degree of stratification is visible in the indicator class simulations (sets 1, 2, and 3) (Figure 10), profiles of  $d_{10}$  values generated in this way are visually similar to those generated directly using SGS (reference set). In sets 1, 2, and 3,  $d_{10}$  values have been assigned randomly from overlapping probability distributions associated with individual indicator classes (Figure 8b), which results in a spatial randomization of  $d_{10}$  values. The similarity of SGS and SIS  $d_{10}$  profiles thus results from (1) the decomposition of the essentially monomodal, nonuniform global  $d_{10}$  probability density function (pdf) (Figure 8a) into subsidiary distributions with smaller, overlapping ranges (Figure 8b); followed by (2) the subsequent reformulation of the global pdf through random sampling of  $d_{10}$  values from the subsidiary pdfs in proportion to the global frequency of occurrence of each subsidiary set. As expected, both the SGS and SIS realizations reproduce the global  $d_{10}$  histogram with fidelity. Profiles generated with the two-step SIS approach are able to preserve additional information regarding the distribution of grain size distribution classes embedded within the indicator class distribution, however.

[38] The uniform porosity assumption results in a direct correlation between  $d_{10}$  and  $K$  values in simulation sets 1 and 2. Independent simulation of a variable porosity field contributes to greater spatial disorder within  $K$  fields estimated using equation (10) in sets 3 and 4, however.

[39] Leverett scaling of air-water entry pressures in the reference and simulation sets 1 and 2 leads to a direct correlation between  $P_b$  and  $K$  values (Figure 11a). This inverse relationship is also apparent in the inversion of light and dark pixels within the  $P_b$  and  $K$  fields depicted in Figure 10. The shape of the representative  $P_c$ -Sat curve, as represented by the Brooks-Corey  $\lambda$  value, remains spatially invariant in the reference and simulation sets 1 and 2 (Figure 11b). In contrast, set 3 contains spatially variable  $\lambda$  and  $P_b$  values that are strongly correlated with the distribution of indicator classes (Figure 10). Furthermore, because  $P_b$  is now a function of both porosity and indicator class, a clear correlation between  $P_b$  and  $K$  values is not present (Figure 12a) and Brooks-Corey  $\lambda$  values in set 3 cluster into six groups associated with the six indicator classes (Figure 12b). Although Figure 12a shows more scatter in  $P_b$  versus  $k$  values for set 3 than the corresponding plot in Figure 11a, the spatial arrangement  $P_b$  values in set 3 is more highly correlated (Figure 10), reflecting the

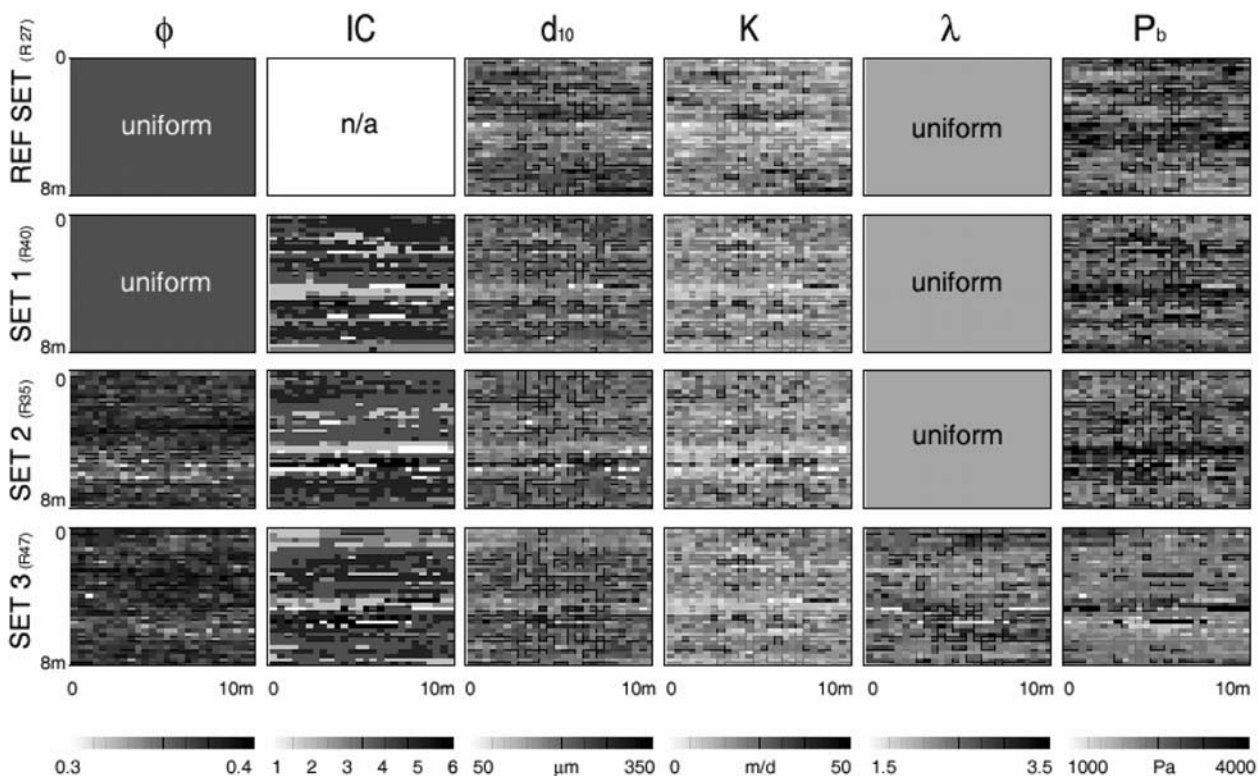


**Figure 10.** Comparison of aquifer parameter distributions in representative two-dimensional profiles extracted from three-dimensional geostatistical simulations. The abbreviation IC stands for indicator class.

stratification present within the original indicator class simulations.

**5.2. Simulated DNAPL Distributions**

[40] Ensemble statistics for saturation, vertical infiltration, and lateral spreading are presented in Table 5 for all simulation sets. Figure 13 illustrates simulated PCE saturations for three representative realizations from each of the four sets. Here realizations generating the minimum, max-

imum, and value closest to the mean of  $\sigma_{xx}^2$  were chosen to represent each set, and PCE saturation is scaled from 0.0001 to 0.05 to enhance the depiction of low saturation variability. Maximum PCE saturations ranged from 0.17 to 0.915 (Table 5) but saturations exceeding 5% occurred in fewer than 3% of the cells containing PCE in each model. Note that the maximum liquid organic saturation in each simulation was limited to 0.915 by the assumed irreducible water saturation of 0.085. Across all realizations, the

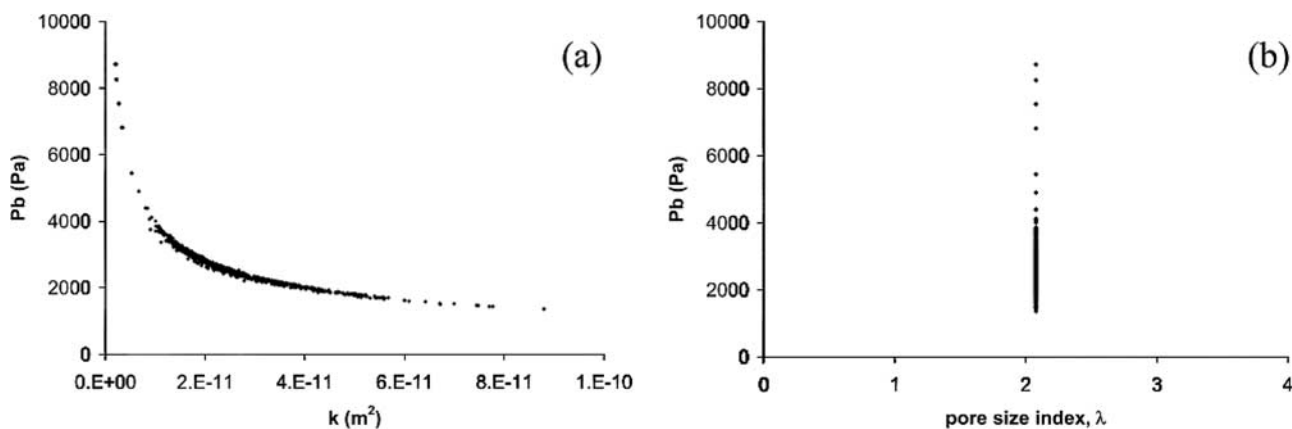


**Figure 11.** Cross plots of (a)  $P_b$  versus  $k$  and (b)  $P_b$  versus  $\lambda$  for realization 2 of simulation set 2. Leverett scaling of the entry pressure from a single representative  $P_c$ -Sat curve results in a direct correlation between  $P_b$  and  $k$  as well as very high entry pressures for low-permeability cells. Adoption of a single representative  $P_c$ -Sat curve also imposes a single value for the pore size distribution (shape) factor,  $\lambda$ , across all  $P_b$  values.

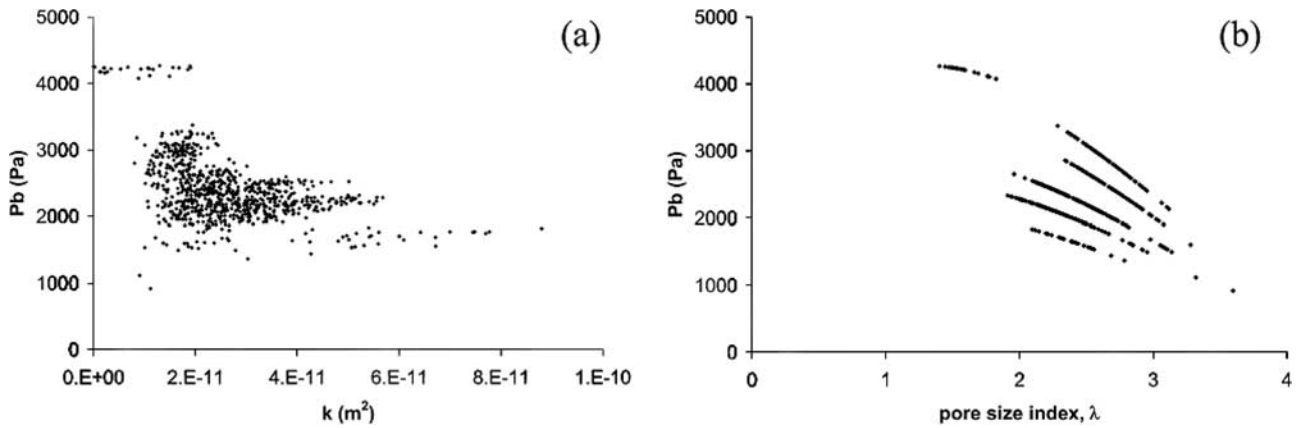


**Figure 12.** Cross plots of (a)  $P_b$  versus  $k$  and (b)  $P_b$  versus  $\lambda$  for realization 2 of simulation set 3.  $P_b$  and  $\lambda$  values were assigned using the Haverkamp and Parlange method on the basis of nodal porosity values and the representative grain size curve corresponding to the nodal indicator class (Figure 9).

average saturation of cells containing PCE at saturations greater than the specified M-VALOR convergence criterion of  $1.0 \times 10^{-4}$  ranged from 0.01 to 0.04, with the greatest variability occurring in set 3. These values are consistent with measured organic liquid saturations reported by *Poulsen and Kueper* [1992] for a field experiment involving the release of tetrachloroethylene into an unsaturated fine to medium grained sand located at Canadian Forces Base Borden in Ontario. PCE saturation profiles and ensemble statistics from set 3 consistently differ from those of the first three simulation sets (Table 5). Set 3 simulations showed little variance in maximum PCE saturations, an overall increase in vertical penetration ( $z_{cm}$ ), and a decreased degree of lateral spreading ( $\sigma_{xx}^2$ ). Maximum  $P_b$  values in simulation sets employing Leverett scaling are significantly higher than those in set 3 (Figures 11 and 12) and may contribute to the tendency for greater lateral spreading in the reference set and sets 1 and 2. Despite lower maximum entry pressures, realizations in set 3 exhibit maximum organic liquid saturation values approaching the limiting value of  $1-S_{wr}$ . Analysis of the high saturation cells in set 3 output files suggests that apparent pooling in these simulations is caused by entry pressure contrast rather than contrast in  $k$  values.

## 6. Discussion

[41] This study examined the influence of four alternative approaches to characterizing aquifer parameter spatial variability in a statistically homogeneous but nonuniform sand aquifer. Comparison of predicted entrapped PCE distributions for the four approaches considered reveals that modeling choices involving the representation of permeability or porosity have a smaller influence than choices involving the scaling of capillary retention properties to  $k$ . In general, ensemble behavior is similar in the reference set and sets 1 and 2, although greater variability in the distribution of PCE saturation is observed in set 2 relative to set 1 due to the additional independent porosity variation incorporated into set 2.

[42] Even though simulation sets 2 and 3 share identical porosity and permeability distributions, set 3 exhibits markedly different PCE spreading and pooling behavior, which is

mainly attributable to the assignment of  $P_c$ -Sat parameters independently of the intrinsic permeability field. Leverett scaling in the reference and simulation sets 1 and 2 leads to a direct correlation between  $P_b$  and  $k$  (Figure 11a) while the absence of Leverett scaling in set 3 decreases this dependency (Figure 12a). Cross plots of  $P_b$  and  $\lambda$  (Figure 12b) show that HPM generated  $P_c$ -Sat parameter values are segregated according to grain size distribution classes in set 3 realizations. In this instance, the correlation of  $P_b$  with grain size classes leads to a preservation of the spatial continuity of similar values for air entry pressures (Figure 10) that accounts for the significantly different DNAPL infiltration behavior in set 3. It appears that the lateral juxtaposition of cells containing similar entry pressure values is more important than the presence of a few cells with extreme high entry pressures.

[43] An important motivation for the modeling of NAPL infiltration and entrapment is the need to derive realistic models of organic liquid distribution within DNAPL source

**Table 5.** Ensemble Statistics for PCE Distribution Metrics

Property	Set	Minimum	Mean	Maximum	Standard Deviation
$S_o$ average	R <sup>a</sup>	0.013	0.017	0.028	0.0027
$S_o$ average	1	0.014	0.017	0.021	0.0015
$S_o$ average	2	0.014	0.017	0.023	0.0018
$S_o$ average	3	0.012	0.019	0.039	0.0060
$S_o$ maximum	R	0.172	0.355	0.625	0.086
$S_o$ maximum	1	0.210	0.358	0.501	0.080
$S_o$ maximum	2	0.198	0.370	0.567	0.086
$S_o$ maximum	3	0.900	0.910	0.915	0.004
$\sigma_{xx}^2$	R	0.273	0.663	1.722	0.295
$\sigma_{xx}^2$	1	0.263	0.530	2.177	0.284
$\sigma_{xx}^2$	2	0.227	0.545	2.550	0.320
$\sigma_{xx}^2$	3	0.174	0.433	0.868	0.166
$z_{cm}$	R	2.583	3.639	4.611	0.472
$z_{cm}$	1	2.638	3.569	4.233	0.303
$z_{cm}$	2	2.871	3.532	4.450	0.302
$z_{cm}$	3	2.220	4.318	6.012	1.050
$\sigma_{zz}^2$	R	2.193	4.418	7.856	1.367
$\sigma_{zz}^2$	1	2.459	4.117	6.112	0.909
$\sigma_{zz}^2$	2	2.417	4.157	7.476	0.971
$\sigma_{zz}^2$	3	0.648	4.202	9.551	2.311

<sup>a</sup>R refers to the reference set.

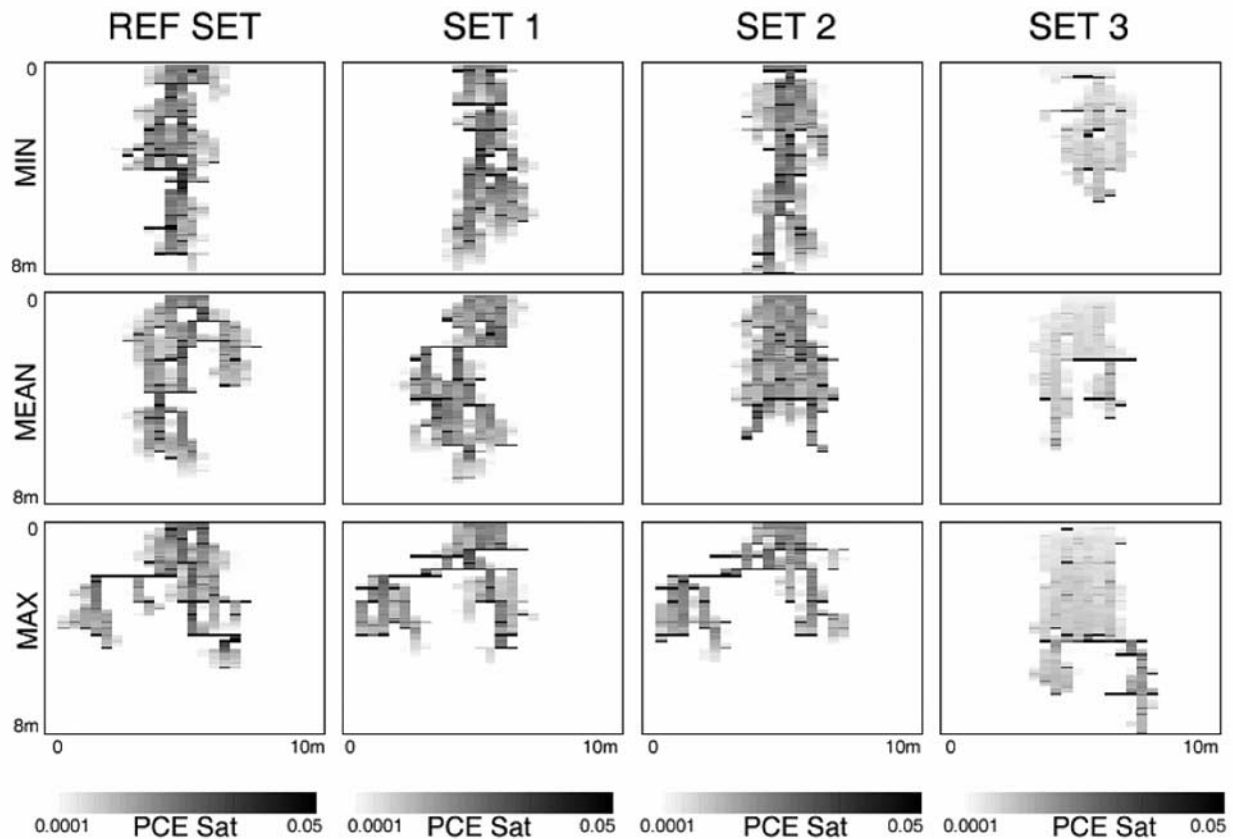


**Figure 13.** Representative DNAPL saturation distributions for each simulation set. Realizations were selected to illustrate minimum, mean, and maximum spreading as measured by the second spatial moment about the  $x$  axis center of mass,  $\sigma_{xx}^2$ .

zones for use in pre- and post-remediation contaminant mass flux estimation. Mathematical modeling suggests that DNAPL source zone architecture will govern mass transfer and organic source persistence in aquifers with uniform flow fields [Sale and McWhorter, 2001]. Because of the contrast in the magnitude and spatial distribution of predicted maximum organic saturations in the simulation sets incorporating Leverett scaling relative to those that did not, it is anticipated that predicted dissolved contaminant effluent concentrations and response to simulated NAPL remediation technologies will differ using results generated with Leverett scaling compared to those without. It is important, then, to assess which approach generates more realistic source zone representations.

[44] Profiles from all of the simulation sets display irregular downward migration paths or channeling of PCE due to incorporation of macroscopic parameter variations of the type discussed by Kueper and Frind [1991a]. Experimental NAPL release and infiltration into sandboxes packed with cells of contrasting grain size, permeability, and  $P_c$ -Sat characteristics have also demonstrated irregular NAPL migration paths, pooling, and spreading resulting from interfaces between sand cells [e.g., Kueper et al., 1989; Barth, 1999]. Qualitatively, this behavior is consistent with conceptual DNAPL source zone models consisting of fingers of DNAPL entrapped at residual saturation and

pools [Mercer and Cohen, 1990; Anderson et al., 1992; Sale and McWhorter, 2001]. Increased spill rates can lead to higher organic liquid saturations and decreased spreading [Kueper and Gerhard, 1995; Dekker and Abriola, 2000a]. Simulated PCE release at rates higher than those used in this investigation (e.g., for a catastrophic spill) could result in higher maximum PCE saturations in ensembles employing Leverett scaling and higher overall saturations in all ensembles, potentially masking differences among the alternative spatial variability modeling approaches investigated herein.

[45] Although all of the simulation sets are qualitatively consistent with DNAPL source zone conceptual models, the procedure used to generate set 3 may be more representative of the aquifer for two reasons. First, the assumption of perfectly correlated entry pressure and permeability fields may be limiting. Published data on the correlation of aquifer conductivity and retention data are sparse; however, both Russo and Bouton [1992] and Hills et al. [1992] found very poor correlations ( $r^2 < 0.25$ ) between the log of measured values for saturated hydraulic conductivity and the van Genuchten  $\alpha$  parameter in analyses involving 400 to 600 in situ and undisturbed soil samples. Second, although both the SGS and SIS approaches were able to replicate the overall  $d_{10}$  histogram, use of the SIS method captures more information from the original data set. Specifically, the

spatial variability in contrasting grain size distribution curve shapes is represented in the distribution of geostatistical indicator classes. In nonuniform sands, the correlation between the shape of particle size distribution and pore size distribution is strong, leading to the ability to estimate  $P_c$ -Sat characteristics from grain size distribution curves. Assignment of  $P_c$ -Sat parameters on the basis of indicator class distribution preserves the simulated spatial continuity of the indicator classes, taking advantage of the GSD information embedded within those classes. Conversely, if a representative retention curve is scaled to permeability, the  $P_b$  field is mapped onto the structure of the  $k$  field and NAPL spreading phenomena related to the lateral continuity of vertically contrasting entry pressure values will be restricted to spatial locations with continuity in vertically dissimilar  $k$  values.

[46] A practical distinction between these two alternative approaches to entry pressure assignment is manifest in the presence and continuity of saturations exceeding 0.60 in set 3 realizations. Field and laboratory measurements of entrapped NAPL saturations for comparison are few, however. The ability to sample NAPL pools at contaminated field sites is difficult, even when their existence can be inferred, because the large number of boreholes required to sample small NAPL pools is often cost prohibitive [Feenstra et al., 1996]. Because of NAPL toxicity and the difficulty in deconstructing sandbox experiments, laboratory measurements of NAPL saturation are also problematic. Therefore a lack of reported high saturation values might not be indicative of the full range of in situ NAPL saturations that are possible under field and laboratory conditions. Nevertheless, saturations exceeding 0.60 are consistent with values reported by Essaid et al. [1993], Dillard et al. [1997], and Barth [1999]. Others reported saturations approaching 0.38 in the field [Kueper et al., 1993] and 0.50 in the lab [Kueper et al., 1989].

[47] The results of this set of numerical simulations demonstrate that independent variation in more than one aquifer parameter can increase the variance of model performance metrics (e.g., observed spreading). For statistically homogeneous, nonuniform sand aquifers, the choice between parametric and nonparametric (SGS vs. SIS) approaches to modeling the spatial distribution of  $k$  or  $\ln(K)$  has only a minor influence on predicted DNAPL distributions if  $P_c$ -sat parameter scaling to  $k$  is also employed. Similarly, the choice between uniform and spatially variable porosity has a relatively small effect. However, assignment of alternative  $P_c$ -Sat indices based on spatially-correlated grain size classes can have a significant influence on predicted DNAPL distributions. This contrast in predicted DNAPL distributions is expected to result in differing behavior with respect to contaminant mass flux and remediation efficiency. Differences in contaminant recovery and mass flux resulting from these alternatives models will be explored in a subsequent paper.

[48] **Acknowledgments.** The U.S. Environmental Protection Agency, Great Lakes and Mid-Atlantic Center for Hazardous Substance Research (GLMAC-HSRC) under grant R-825540, the Michigan Department of Environmental Quality (MDEQ) under contract Y80011, and the Strategic Environmental Research and Development Program (SERDP) under contract CU-1293 provided funding for this research. The content of this publication has not been subject to agency review and does not necessarily represent the views of agency sponsors. This paper was improved

by the thoughtful comments and questions provided by two anonymous reviewers.

## References

- Abriola, L. M., K. M. Rathfelder, S. Yadav, and M. Maiza (1992), VALOR code version 1.0: A PC code for simulating subsurface immiscible contaminant transport, *Rep. EPRI TR-101018*, Electric Power Res. Inst., Palo Alto, Calif.
- Anderson, M. R., R. L. Johnson, and J. F. Pankow (1992), Dissolution of dense chlorinated solvents into groundwater: 3. Modeling contaminant plumes from fingers and pools of solvent, *Environ. Sci. Technol.*, **26**, 901–908.
- Arya, L. M., and T. S. Dierolf (1992), Predicting soil moisture characteristics from particle size distributions; an improved method to calculate pore radii from particle radii, in *Proceedings of the International Workshop on Indirect Methods for Estimating the Hydraulic Properties of Unsaturated Soils*, edited by M. T. van Genuchten, F. J. Leij, and L. J. Lund, pp. 115–124, Univ. of Calif., Riverside.
- Arya, L. M., and J. F. Paris (1981), A physicoempirical model to predict the soil moisture characteristic from particle-size distribution and bulk density analysis, *Soil Sci. Am. J.*, **45**, 1023–1030.
- Barth, G. R. (1999), Intermediate-scale tracer tests in heterogeneous porous media: Investigation of density, predictability and characterization of NAPL entrapment (subsurface solute transport), Ph.D. thesis, Univ. of Colo., Boulder.
- Bear, J. (1972), *Dynamics of Fluids in Porous Media*, Elsevier Sci., New York.
- Brooks, R. H., and A. T. Corey (1964), Hydraulic properties of porous media, *Hydrol. Pap. 3*, Colo. State Univ., Fort Collins.
- Burdine, N. T. (1953), Relative permeability calculations from pore size distribution data, *Trans. Am. Inst. Min. Metall. Pet. Eng.*, **198**, 71–78.
- Chen, J., J. W. Hopkins, and M. E. Grismer (1999), Parameter estimation of two-fluid capillary pressure-saturation and permeability functions, *Adv. Water Resour.*, **22**, 479–493.
- Dekker, T. J., and L. M. Abriola (2000a), The influence of field scale heterogeneity on the infiltration and entrapment of dense nonaqueous phase liquids in saturated formations, *J. Contam. Hydrol.*, **42**, 187–218.
- Dekker, T. J., and L. M. Abriola (2000b), The influence of field scale heterogeneity on the surfactant-enhanced remediation of entrapped nonaqueous phase liquids, *J. Contam. Hydrol.*, **42**, 219–251.
- Demond, A. H., and P. V. Roberts (1987), An examination of relative permeability relations for two-phase flow in porous media, *Water Resour. Bull.*, **23**, 617–628.
- Demond, A. H., K. M. Rathfelder, and L. M. Abriola (1996), Simulation of organic liquid flow in porous media using estimated and measured transport properties, *J. Contam. Hydrol.*, **22**, 223–239.
- Deutsch, C. V., and A. G. Journel (1998), *Geostatistical Software Library and User's Guide*, 2nd ed., Oxford Univ. Press, New York.
- Dillard, L. A., H. I. Essaid, and W. N. Herkelrath (1997), Multiphase flow modeling of a crude-oil spill site with a bimodal permeability distribution, *Water Resour. Res.*, **33**, 1617–1632.
- Dominic, D. F., R. W. Ritzi Jr., E. C. Reboulet, and A. C. Zimmer (1998), Geostatistical analysis of facies distributions: Elements of a quantitative facies model, in *Hydrogeologic Models of Sedimentary Aquifers*, edited by G. S. Fraser and M. J. Davis, pp. 137–146, Soc. for Sediment. Geol., Tulsa, Okla.
- Drummond, C. D., L. D. Lemke, K. M. Rathfelder, E. J. Hahn, and L. M. Abriola (2000), Simulation of surfactant-enhanced PCE recovery at a pilot test field site, in *Treating Dense Nonaqueous Phase Liquids (DNAPLs): Remediation of Chlorinated and Recalcitrant Compounds*, edited by G. B. Wickramanayake, A. R. Gavaskar, and N. Gupta, pp. 77–84, Batelle, Columbus, Ohio.
- Essaid, H. I., and K. M. Hess (1993), Monte Carlo simulations of multiphase flow incorporating spatial variability of hydraulic properties, *Ground Water*, **31**, 123–134.
- Essaid, H. I., W. N. Herkelrath, and K. M. Hess (1993), Simulation of fluid distributions observed at a crude oil spill site incorporating hysteresis, oil entrapment, and spatial variability of hydraulic properties, *Water Resour. Res.*, **29**, 1753–1770.
- Feenstra, S., J. A. Cherry, and B. L. Parker (1996), Conceptual models for the behavior of dense non-aqueous phase liquids (DNAPLs) in the subsurface, in *Dense Chlorinated Solvents and Other DNAPLs in Groundwater: History, Behavior, and Remediation*, edited by J. F. Pankow and J. A. Cherry, chap. 2, Waterloo, Portland, Oreg.

- Fountain, J. C. (1997), Removal of nonaqueous phase liquids using surfactants, in *Subsurface Restoration*, edited by C. H. Ward, J. A. Cherry, and M. R. Scaif, pp. 199–207, Ann Arbor Press, Chelsea, Mich.
- Fountain, J. C., R. C. Starr, T. Middleton, M. Beikirch, C. Taylor, and D. Hodge (1996), Controlled field test of surfactant-enhanced aquifer remediation, *Ground Water*, 34, 910–916.
- Freeze, R. A. (1975), A stochastic-conceptual analysis of one-dimensional groundwater flow in nonuniform homogeneous media, *Water Resour. Res.*, 11, 725–741.
- Goggin, D. J., and D. L. Jordan (1995), The use of categorical indicator geostatistics for modeling facies in sand-rich turbidite systems; an example from the deep-water Gulf of Mexico, *AAPG Bull.*, 79, 1216.
- Gomez-Hernandez, J. J. (1997), Issues on environmental risk assessment, in *Geostatistics Wollongong '96*, vol. 1, edited by E. Y. Baafi and N. A. Schofield, pp. 15–26, Kluwer Acad., Norwell, Mass.
- Gomez-Hernandez, J. J., and X.-H. Wen (1998), To be or not to be multi-Gaussian? A reflection on stochastic hydrology, *Adv. Water Resour.*, 21, 46–61.
- Goovaerts, P. (1997), *Geostatistics for Natural Resources Evaluation*, Oxford Univ. Press, New York.
- Goovaerts, P. (1998), Geostatistical tools for characterizing the spatial variability of microbiological and physico-chemical soil properties, *Biol. Fertil. Soils*, 27, 315–334.
- Goovaerts, P. (1999), Impact of the simulation algorithm, magnitude of ergodic fluctuations and number of realizations on the spaces of uncertainty of flow properties, *Stochastic Environ. Res. Risk Assess.*, 13, 161–182.
- Greenkorn, R. A., and D. P. Kessler (1969), Dispersion in heterogeneous nonuniform anisotropic porous media, *Ind. Eng. Chem.*, 61, 14–32.
- Haverkamp, R., and J. Y. Parlange (1986), Predicting the water-retention curve from particle-size distribution: 1. Sandy soils without organic matter, *Soil Sci.*, 142, 325–339.
- Hess, K. M., S. H. Wolf, and M. A. Celia (1991), Estimation of macro-dispersivities from the spatial variability of hydraulic conductivity in a sand and gravel aquifer, Cape Cod, Massachusetts, *U.S. Geol. Surv. Water Resources Invest. Rep.*, 91-4034, 15–21.
- Hills, R. G., D. B. Hudson, and P. J. Wierenga (1992), Spatial variability at the Las Cruces trench site, in *Proceedings of the International Workshop on Indirect Methods for Estimating the Hydraulic Properties of Unsaturated Soils*, edited by M. T. van Genuchten, F. J. Leij, and L. J. Lund, pp. 529–538, Univ. of Calif., Riverside.
- Johnson, N. M. (1995), Characterization of alluvial hydrostratigraphy with indicator semivariograms, *Water Resour. Res.*, 31, 3217–3227.
- Johnson, N. M., and S. J. Dreiss (1989), Hydrostratigraphic interpretation using indicator geostatistics, *Water Resour. Res.*, 25, 2501–2510.
- Journel, A. G., and C. V. Deutsch (1993), Entropy and spatial disorder, *Math. Geol.*, 25, 329–355.
- Journel, A. G., and C. J. Huijbregts (1978), *Mining Geostatistics*, Academic, San Diego, Calif.
- Kaluarachchi, J. J., and J. C. Parker (1992), Multiphase flow with a simplified model for oil entrapment, *Transp. Porous Media*, 7, 1–14.
- Koltermann, C. E., and S. M. Gorelick (1995), Fractional packing model for hydraulic conductivity derived from sediment mixtures, *Water Resour. Res.*, 31, 3283–3297.
- Koltermann, C. E., and S. M. Gorelick (1996), Heterogeneity in sedimentary deposits: A review of structure-imitating, process-imitating and descriptive approaches, *Water Resour. Res.*, 32, 2617–2658.
- Kueper, B. H., and E. O. Frind (1991a), Two-phase flow in heterogeneous porous media: 1. Model development, *Water Resour. Res.*, 27, 1049–1057.
- Kueper, B. H., and E. O. Frind (1991b), Two-phase flow in heterogeneous porous media: 2. Model application, *Water Resour. Res.*, 27, 1059–1070.
- Kueper, B. H., and J. I. Gerhard (1995), Variability of point source infiltration rates for two-phase flow in heterogeneous porous media, *Water Resour. Res.*, 31, 2971–2980.
- Kueper, B. H., W. Abbott, and G. Farquhar (1989), Experimental observations of multiphase flow in heterogeneous porous media, *J. Contam. Hydrol.*, 5, 83–95.
- Kueper, B. H., D. Redman, R. C. Starr, S. Reitsma, and M. Mah (1993), A field experiment to study the behavior of tetrachloroethylene below the water table: Spatial distribution of residual and pooled DNAPL, *Ground Water*, 31, 756–766.
- Kupfersberger, H., and C. V. Deutsch (1999), Methodology for integrating analog geologic data in 3-D variogram modeling, *AAPG Bull.*, 83, 1262–1278.
- Land, C. S. (1968), Calculation of imbibition relative permeability for two- and three-phase flow from rock properties, *Soc. Pet. Eng. J.*, 8, 149–156.
- Lemke, L. D. (2003), Influence of alternative spatial variability models on solute transport, DNAPL entrapment, and DNAPL recovery in a homogeneous, nonuniform sand aquifer, Ph.D. thesis, Univ. of Mich., Ann Arbor.
- Lenhard, R. J., J. C. Parker, and J. J. Kaluarachchi (1991), Comparing simulated and experimental hysteretic two-phase transient fluid flow phenomena, *Water Resour. Res.*, 27, 2113–2124.
- Leverett, M. C. (1941), Capillary behavior in porous solids, *Pet. Dev. Technol.*, 142, 152–169.
- Mercer, J. W., and R. M. Cohen (1990), A review of immiscible fluids in the subsurface: Properties, models, characterization, and remediation, *J. Contam. Hydrol.*, 6, 107–163.
- Meyers, J. C. (1997), *Geostatistical Error Management: Quantifying Uncertainty for Environmental Sampling and Mapping*, Van Nostrand Reinhold, New York.
- National Research Council (1994), *Alternatives for Groundwater Cleanup*, Natl. Acad. Press, Washington, D. C.
- Parker, J. C., and R. J. Lenhard (1987), A model for hysteretic constitutive relations governing multiphase flow: 1. Saturation-pressure relations, *Water Resour. Res.*, 23, 2187–2196.
- Poeter, E., and P. Townsend (1990), Multiple indicator conditional stochastic simulation of a section of the unconfined aquifer, Hanford Site, Washington, USA, in *Fifth Canadian/American Conference on Hydrogeology*, edited by B. Hitchon, pp. 159–188, Natl. Water Well Assoc., Banff, Alberta, Canada.
- Poulsen, M. M., and B. H. Kueper (1992), A field experiment to study the behavior of tetrachloroethylene in unsaturated porous media, *Environ. Sci. Technol.*, 26, 889–895.
- Ptak, T. (1997), Evaluation of reactive transport processes in a heterogeneous porous aquifer within a non-parametric numerical stochastic transport modeling framework based on sequential indicator simulation of categorical variables, in *geoENV I—Geostatistics for Environmental Applications*, edited by A. Soares et al., pp. 153–165, Kluwer Acad., Norwell, Mass.
- Rathfelder, K. M., and L. M. Abriola (1998), Influence of capillarity in numerical modeling of organic liquid redistribution in two-phase systems, *Adv. Water Resour.*, 21, 159–170.
- Rathfelder, K. M., L. M. Abriola, M. A. Singletary, and K. D. Pennell (2003), Influence of surfactant-facilitated interfacial tension reduction on chlorinated solvent migration in porous media: Observations and numerical simulation, *J. Contam. Hydrol.*, 64(3–4), 227–252, doi:10.1016/S0169-7722(02)00205-X.
- Ritzi, R. W., Jr., D. F. Dominic, N. R. Brown, K. W. Kausch, P. J. McAlleney, and M. J. Basial (1995), Hydrofacies distribution and correlation in the Miami Valley aquifer system, *Water Resour. Res.*, 31, 3271–3281.
- Rubin, Y., and A. G. Journel (1991), Simulation of non-Gaussian space random functions for modeling transport in groundwater, *Water Resour. Res.*, 27, 1711–1721.
- Russo, D., and M. Bouton (1992), Statistical analysis of spatial variability in unsaturated flow parameters, *Water Resour. Res.*, 28, 1911–1925.
- Saenton, S., T. H. Illangasekare, K. Soga, and T. A. Saba (2002), Effects of source zone heterogeneity on surfactant-enhanced NAPL dissolution and resulting remediation end-points, *J. Contam. Hydrol.*, 59, 27–44.
- Sale, T. C., and D. B. McWhorter (2001), Steady state mass transfer from single-component dense nonaqueous phase liquids in uniform flow fields, *Water Resour. Res.*, 37, 393–404.
- Salehzadeh, A., and A. H. Demond (1999), Pressure cell for measuring capillary pressure relationships of contaminated sands, *J. Environ. Eng.*, 125, 385–388.
- Schad, H. (1993), Geostatistical analysis of hydraulic conductivity related data based on core samples from a heterogeneous fluvial aquifer, in *Statistics of Spatial Processes: Theory and Applications*, edited by C. Vincenzo, G. Giovanni, and P. Donato, pp. 205–212, It. Stat. Soc., Bari, Italy.
- Srivastava, R. M. (1994), An overview of stochastic methods for reservoir characterization, in *Stochastic Modeling and Geostatistics: Principles, Methods, and Case Studies*, edited by J. M. Yarus and R. L. Chambers, pp. 1–16, Am. Assoc. of Pet. Geol., Tulsa, Okla.
- Strategic Environmental Research and Development Program and Environmental Security Technology Certification Program (2002), SERDP/ESTCP expert panel workshop on research and development needs for

- cleanup of chlorinated solvent sites, final report, Strategic Environ. Res. and Dev. Program, Arlington, Va.
- Van Geel, P. J., and J. F. Sykes (1994), Laboratory and model simulations of a LNAPL spill in a variably-saturated sand: 2. Comparison of laboratory and model results, *J. Contam. Hydrol.*, 17, 27–53.
- van Genuchten, M. T. (1980), A closed-form equation for predicting the hydraulic conductivity of unsaturated soils, *Sci. Soc. Am. J.*, 44, 892–898.
- Wilson, J. L., S. H. Conrad, W. R. Mason, W. Peplinski, and E. Hagan (1990), Laboratory investigations of residual liquid organics from spills, leaks and disposal of hazardous wastes in groundwater, *Rep. EPA/600/6-90/004*, U.S. Environ. Prot. Agency, Ada, Okla.
- Woodbury, A. D., and E. A. Sudicky (1991), The geostatistical characterization of the Borden aquifer, *Water Resour. Res.*, 27, 533–546.
- 
- L. M. Abriola, Department of Civil and Environmental Engineering, University of Michigan, Ann Arbor, MI 48109, USA.
- P. Goovaerts, Biomedware, Inc., 516 North State Street, Ann Arbor, MI 48104, USA.
- L. D. Lemke, Department of Geology, Wayne State University, Detroit, MI 48202, USA. (ldlemke@wayne.edu)